

International Jour	nal of Compu	ıtational N	<b>laterials</b>
--------------------	--------------	-------------	------------------

- Science and Engineering
- § (2022) 2250015 (16 pages)
- 4 @ World Scientific Publishing Europe Ltd.
- 5 DOI: 10.1142/S2047684122500154

9 Chi Ma\*, Huan Zhaot and Yan Li\* 10 Thayer School of Engineering, Dartmouth College, Hanover NH 03755, 11 12 \*chi.ma@dartmou.th.edu thuan.zhao.th@dartmouth.edu 13 \*yan.li@dartmou.th.edu 14 15 Received 5 May 2022 Revised 16 June 2022 16 Accepted 22 June 2022 17 Published 18

Polymer-derived ceramics (PDCs) which are fabricated through pyrolysis of preceramic polymers have attracted increasing attention due to their versatility in structure architecture design and property tailoring. Shaping at the polymer state using 3D printing allows the final ceramic products to exhibit arbitrary shapes and complex architectures that areotherwise impossible to achieve through traditional processing routes. The polymer-to-ceramic phase transition also provides additional space for mechanical property tailoring. A multiscale computational model is developed to explore the phase transition mechanisms and their correlations with processing parameters and failure response. Calculations in this work concern PMHS/DVB preceramic polymers. Molecular dynamics (MD) simulations are carried out first to track the atomic structure evolution at different temperatures. Continuum-scale ceramic phase formation is calculated on the basis of the competition between gas generation and gas diffusion. The effect of processing parameters on mechanical properties of pyrolyzed PMHS/DVB is systematicallystudied. Conclusions from this study can provide direct guidance for fabricating PDC composites with tailored mechanical properties.

Keywords: Polymer-derived ceramics (PDCs); phase transition analysis; finite element simulation.

#### 1. Introduction

19

20

21

23

24

25

26 27

29 30

31

32 33

35

37

38

39

40

41

Advanced ceramics represent a key enabling technology in aerospace, defense, power generation, and healthcare industries due to their superior properties, such as lightweight [Alizadeh-Osgouei *et al.*, 2018], high strength [Waku *et al.*, 1997], excellent thermal stability [Justin and Jankowiak, 2011] and high corrosion resistance [Wei *et al.*, 2005]. Traditional ceramic processing technique has very little control

<sup>\*</sup>Corresponding author.

2

3

5

6

S

9

10

11

12

13

14

15

16

17

18

19

20

21

22

24

25

27

28

29

30

31

32

33

34

35

36

37

38

40

41

42

over material geometry and does not provide enough room for property tailoring [Gonzalez et al., 2018]. Discovery of polymer-derived ceramics (PDCs) in 1960 has enabled significant technological breakthroughs in cerainic science and technology [Colombo et al., 2009]. This fabrication approach, which converts precerainic polymers to ceramics through heat treatment under an inert or reacting atmosphere, opens up new opportunities for property tailoring through phase transition control [Gottardo et al., 2012; Soraru. et al., 2019; Wan et al., 2004]. Recently, additive manufacturing technology has enabled fabrication of preceramic polymers with complex shapes and architectures [Eckel et al., 2016; Konstantinou et al., 2020]. Shaping at the polymer state not only avoids problems related to tool wear and brittle fracture upon finishing the ceramic component, but also provides new opportunities for geometric design which is of great importance in applications, such as custoinized biomedical implants, body armor, and energy storage devices, etc. Understanding the effect of key processing parameters on mechanical properties of PDCs requires in-depth understanding of the phase transition process. Experimental characterizations, e.g. thermogravimetric analysis (TGA) [Venkatachalam and Hourlier, 2019] and infrared spectroscopy [Gottardo et al., 2012], can track the mass loss associated with precerainic polymer decomposition during pyrolysis. However, these approaches alone cannot directly reveal the molecular structure evolution which is an important aspect of phase transition. Scanning electron inicroscopy (SEM) and transinission electron inicroscopy (TEM) [Vry et al., 2020], which can provide detailed nano/micro structure characterization, are only available after sample pyrolysis. Computational models can address some of the underlying physics that cannot be directly captured during experiment. Molecular dynamics (MD) models have been employed to simulate the cheinical reaction mechanisms and atoinic structure change during pyrolysis [Lu et al., 2015; Ponomarev et al., 2019]. However, conclusions from MD simulations cannot be directly employed to guide the manufacturing process due to the large time and length scale gaps. Bernard et al. [2006] proposed a diffusion-controlled kinetic model which predicts polymer-to-cerainic phase transition at the structure level. Their prediction of polymer-to-ceramic conversion did not account for the temperature field evolution or the change of heat transfer behavior during the dynamic phase transition process. In fact, the current state phase composition will largely affect the heat transfer behavior and temperature field evolution that will ultimately deterinine the subsequent polymer decomposition and phase redistribution. This is because the thermal conductivity of cerainics is about ten times higher than that of polymers [Stabler et al., 2018]. The thermal conductivity of the entire material tends to increase when the polymer phase is gradually converted to the cerainic phase, leading to more intensified subsequent polymer decomposition. A computational model which finds the inissing link between the atoinic level structure evolution and macroscale phase composition map will promote in-depth understanding of the physics of phase transition process. Additionally, quantitative correlation of processing parameters with mechanical response

of the pyrolyzed preceramic materials will provide a useful roadmap for fabricating PDCs/PDC composites with tailored properties and functionalities. Currently, few computational studies are available to find the systematic correlations, especially when intermediate polymer-ceramic phases are present.

In this paper, a multiscale computational model is developed to study the effect of key pyrolysis parameters on phase transition and mechanical properties of pyrolyzed PMHS/DVB samples. Gas generation during pyrolysis is captured through MD simulations. Continuum-scale phase transition is predicted based on the competition between gas generation and gas diffusion in Sec. 2.1. The constitutive law in the intermediate phase is developed on the basis of the microhardness testing results. The overall mechanical response of the PDC composites is predicted through tension simulation as presented in Sec. 2.2. The effect of heating rate, pyrolysis temperature and holding time on elastic modulus and tensile fracture behavior is systematically studied in Secs. 3.1 and 3.2, respectively. The developed model, which correlates key processing parameters with mechanical response, will reduce the time and cost in developing future PDCs with tailored mechanical properties.

## 2. Model Description

## **2.1.** Multiscale modeling of phase transition

#### 2.1.1. MD simulation on atomic structure evolution

A preceramic polymer system, in which polymethylhydrosiloxane (PMHS) is crosslinked by divinylbenzene (DVB), is modeled in this work. Polymer chains with molar mass of 1500g/mol are first constructed and randomly packed in the simulation box. DVB molecules are bonded to different polymer chains to create the network structure, which is imported to large-scale atomic/molecular massively parallel simulator (LAMMPS) to obtain system equilibrium [Ma et al., 2017b; Plimpton, 1995]. Parameters of reaction force field are selected based on the work of Kulkarni et al. [2013]. Constant temperature and pressure ensemble (NPT) are utilized with a time step of 0.1 fs. The pre-pyrolysis system is equilibrated at 300K as shown in Fig. l(a). The pyrolysis process is simulated by considering a range of pyrolysis temperatures from 873K to 2500K with constant heating rate of 0.1 K/fs and time step of 0.2fs. The top surface of the simulation box is set to move freely along the vertical direction. At the height of three times of the initial box length, the temperature is set to 0.1 K by Berendsen thermostat in order to trap the diffused gas molecules. Periodic boundary conditions are applied to the rest of the surfaces.

Chemical reactions during pyrolysis are elucidated in Fig. 1(b). At a pyrolysis temperature of 1500K, bond breakage occurs to form free radicals (e.g., -CH3) and atoms (e.g. H atoms). Gaseous products, such as H2 and C, argenerated due to the new bond formation. Mass loss occurs as the gaseous products are gradually released out of the system during pyrolysis. In the MD model, mass loss is counted as the overall mass of generated gaseous molecules. As indicated in Fig. 1(c), higher

2

3

7

a

9

10

11

12

13

14

15

16

17

18

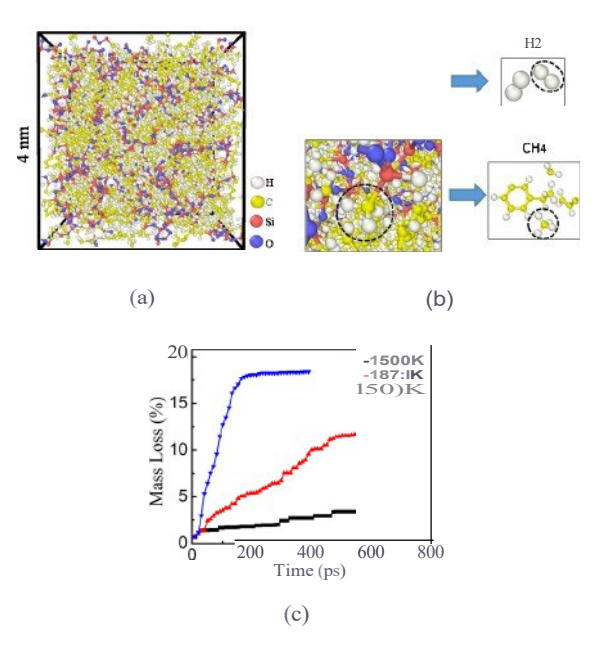


Fig. 1. (a) Equilibrated PMHS/DVB systems before pyrolysis; (b) atomic debonding and rebonding process at 1500 K during pyrolysis; and (c) mass loss at different pyrolysis temperatures.

pyrolysis temperature corresponds to higher amount of mass loss, which is consistent with the TGA [Li *et al.*, 2018a; You *et al.*, 2019]. Additionally, an earlier saturation of mass loss is reached at a higher pyrolysis temperature. It can be inferred that the time required for complete gas generation is 772ps under 1500K, 473ps under 1873K, and 180ps under 2500 K, respectively. Therefore, it is reasonable to consider that gasgeneration occurs instantly at the structure level. The total amount of mass loss only depends on the pyrolysis temperature. The generated gas density '1/;(T) is calculated as

$$'1/;(T) = ffigas(T)PinitiaJ/minitial = 1'(oss(T)Pinitial,$$
 (1)

where Pinitial = 1.21g/cc. mgas(T) is the mass of generated gas products at temperature *T*. minitial is the initial system mass. TJoss(T) is the mass loss ratio which is extracted through the thermogravimetric (TGA) analysis from Li *et al.* [20186]. Here, the gas volume in Eq. (1) is assumed to be constant during the fast gas generation process due to the uniform gas molecule distribution in the system.

## 2.1.2. Finite element simulation of phase transition at the continuum level

Gaseous products, which are generated during pyrolysis, need to release out of the system so that the ceramic structure can be formed. Therefore, phase transition requires in-depth understanding of the interplay between gas generation and gas diffusion. At the structure level, a PDC sample during pyrolysis may include three

10

11

12

13

14

15

16

18

19

20

21

22

23

24

Effect of pyrolysis parameters on mechanical properties of polymer-derived ceramics

phases: polymer phase (phase 1), ceramic phase (phase 2) and intermediate phase with partially decomposed polymers. Due to the huge discrepancy of thermal conductivity in each phase, a non-uniform temperature field is expected when different phases coexist. Gas diffusion is triggered as a result of the gas density gradient. Gas diffusion rate 87//J8t, is calculated as

$$\frac{\partial \psi}{\partial t} = D_{\rm T} \nabla^2 \psi(x, y, z, t). \tag{2}$$

where Dr is the diffusion coefficient from the work of Merkel et al. [2000]. At a given moment during pyrolysis, a selected volume of the sample is either under gas gain or gas loss. Ceramic formation requires 81jJ/8t < 0 when gas loss is activated. The ceramic fraction f is defined as

where 7Prelease is the current gas release density and 7Jmax is the maximum gas density that can be generated in a given unit volume. Calculation of f is carried out through a user subroutine UMATHT in ABAQUS. Details of the algorithm can be found in Ma and Li [2021]. In this study, phase transition analysis is conducted on eight cubic preceramic polymer samples with side dimension of 20—Each sample is pyrolyzed according to the predefined heating rate, pyrolysis temperature and holding times as illustrated in Fig. 2 and summarized in Table 1. Figure 3 illustrates the phase composition evolution in the middle cross-section when a heating rate of 0.63K/s and a pyrolysis temperature of 1273K are considered. It is noted that no fully converted ceramic phase is observed at 1200s and 1360s. No pure preceramic polymer phase exists either. At 1540s, around 40% of the sample has been fully converted to ceramics. Complete ceramization of the entire sample is achieved at 2440s according to the simulation. The developed model, which simulates macroscale phase transition process by accounting for both heat transfer and gas diffusion kinetics, can explicitly resolve the real-time phase composition map in

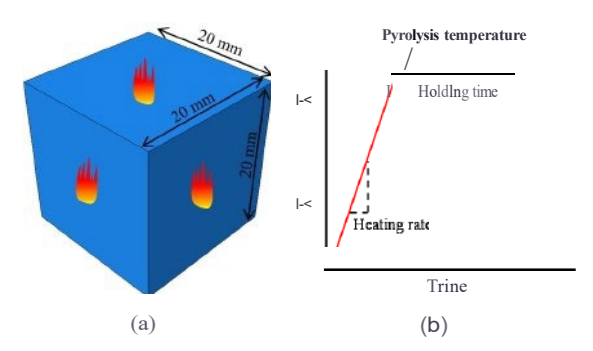


Fig. 2. (a) Scheme of the phase transition model and (b) characterization of key processing parameters.

Table 1. List of samples employed in the phase transition simulations.

Sample number	Heating rate (K/s)	Pyrolysis temperature (K)	Holding time (s)
1	0.63	1273	1200
2	0.63	1273	1360
3	0.63	1273	1540
4	0.17	1273	1200
5	1.26	1273	1200
6	0.63	1273	1700
7	0.63	1473	1700
8	0.63	1673	1700

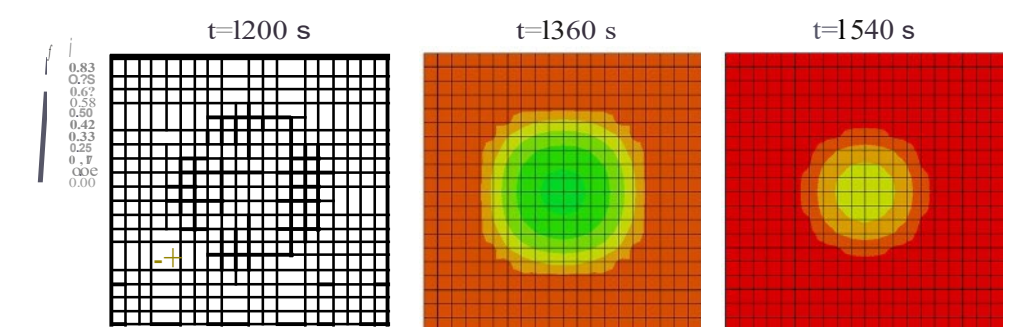


Fig. 3. Phase evolution in the middle cross section at different holding times with heating rate of  $0.63 \, \text{K/s}$  and pyrolysis temperature of  $1273 \, \text{K}$ .

any PDC sample configurations. The phase distribution information will serve as the input for mechanical response prediction in Sec. 2.2.

## 2.2. Mechanical property prediction of pyrolyzed PDC composites

## 2.2.1. Constitutive modeling

2

3

4

10

11

13

14

16

17

18

Different constitutive laws are assigned to the sample based on the phase distribution as illustrated in Fig. 3. In the region where f=0 (Region P), the material is pure preceramic polymer and follows the constitutive relationship that is determined through experiment [Kim *et al.*, 2011]. In the region where f=1 (Region C), the material has been fully converted to the ceramic phase. It follows the isotropic linear elastic constitutive relation with Young's modulus Ee=101 GPa and Poisson's ratio v=0.11. In this work, the intermediate phase (0 < f < 1) is divided into five regions as illustrated in Table 2. According to the discussion in Sec. 2.1, f primarily depends on the pyrolysis temperature T. In order to find the mathematical model of f(T) intheintermediate phase, we prepared a set of PMHS/DVB samples with a mean thickness of 0.615 mm. These samples were pyrolyzed at 873 K, 973 K, 1027 K, 1173 K and 1273 K in a mufll.e furnace, respectively. The mass loss ratio  $T_{\rm Joss}$  is fitted as a function of temperature T as shown in Fig. 4(a). It is noted that  $T_{\rm Joss}$  starts to saturate around 30.3% when T > 1273 K. Below this temperature

Table 2. Region division criterion.

Region name	Ceramic fraction f
Region P	f=0
Region 1	0 20%</td
Region 2	20% 40%</td
Region 3	40%< f 60%
Region 4	60% 80%</td
Region 5	80% < f < 100%
Region C	f = 100%

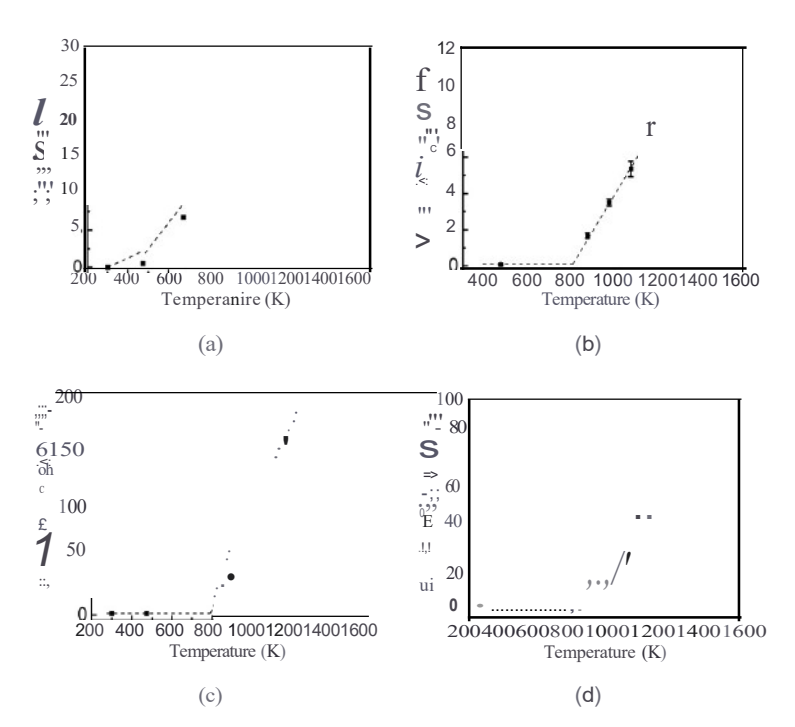


Fig. 4. Relationship of pyrolysis temperature with (a) mass loss ratio, (b) Vickers hardness, (c) ultimate strength and (d) elastic modulus (Kim *et al.*, 2011; Soran) *et al.*, 2019).

threshold, a bilinear mass loss-temperature relationship is found as

$$T(oss(T) = \begin{cases} 1.28 \times 10-41' - 0.0384, & T::; 473K, \\ 3.51 \times 10-41' - 0.1438, & 473K < T::; 1273 K. \end{cases}$$
(4)

According to Eqs. (1) and (3), the ceramic volume fraction f is formulated as

$$f(T) = \begin{cases} 4.22 \times 10 - 41' - 0.1267, & T :: ; 473K, \\ 1.16 \times 10 - 37' - 0.4746, & 473K < T :: ; 1273K. \end{cases}$$
 (5)

2

3

6

9

10

11

12

13

14

15

16

18

19

20

21

22

23

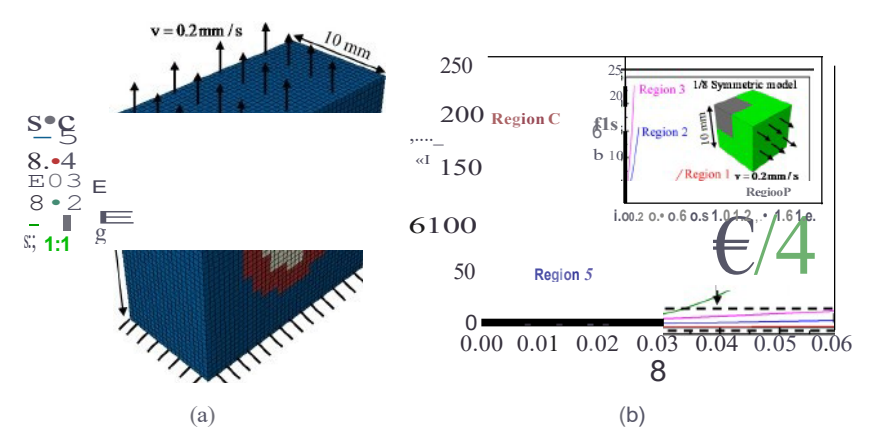


Fig. 5. (a) Sample configuration used in simple tension simulation. Phase composition is extracted at 1360s with pyrolysis temperature of 1273 K and heating rate of 0.63K/s and (b) constitutive relations in different regions.

The ultimate strength auTs is predicted according to

$$auTS(T) = Hv(T)/Const,$$
 (6)

where hardness Hv is measured by applying a 1.96N indentation load on each pyrolyzed sample for 15s using the Wilson Tukon microhardness tester. Const = 21.4 is reported by the existing literature [Vozza, 2021; Zhang  $et\ al.$ , 2011]. According to Figs. 4(b) and 4(c), three linear segments are found from the experiment. The stress-strain relationship of each intermediate region before reaching the ultimate strength is determined from the uniaxial compression simulation as shown in Fig. 5(b). Only 1/8 of the sample is modeled due to symmetry and computational efficiency. The Poisson's ratio of intermediate region i(1 ::::; i ::::; 5) is estimated according to Vi = five + (1 - fi)vp, where Ve = 0.11 and Vp = 0.48 are the Poisson's ratio of pure ceramics (Region C) and preceramic polymers (Region P), respectively. Ji is the averaged ceramic fraction in region i. Figure 5(b) illustrates the stress-strain curve of each region in Table 2. The constitutive relationship is imported to ABAQUS for material property assignment.

# 2.2.2. Prediction of the effective elastic modulus E

As shown in Fig. 5(a), the top surface of the PDC composite sample is subject to a velocity boundary with V = 0.2mm/s, while its bottom surface is fixed. According to the region decomposition criterion in Table 2, region 3, region 4 and region 5 coexist in the sample. The interface between each region can be explicitly delineated as illustrated in Fig. 5(a). The constitutive law of each region is defined according to Sec. 2.2.1. The effective elastic modulus  $\boldsymbol{E}$  of the entire PDC composite sample is evaluated through simple tension simulation. This approach is applied to other PDC composite samples that are pyrolyzed under different pyrolysis parameters. The

- computationally predicted effective elastic modulus is compared with the analytical solution using the Mori-Tanaka (MT) model [Fisher and Brinson, 2006; Lee, 2018;
- Thorvaldsen, 2015]. In the MT model, the effective stiffness tensor C is formulated as

$$C = A_0 \left[ \left( 1 - \sum_{i=1}^{7} v_i \right) C_{\text{polymer}} + \sum_{i=1}^{7} v_i C_i A_i^{\text{dil}} \right], \tag{7}$$

- 4 where  $C_{polymer}$  is the polymer stiffness tensor;  $V_i$  and  $C_i$  are the volume fraction
- and stiffness tensor of region i; Ao and  $At^1$  are the strain concentration factors
- 6 following the following expressions as

$$A_0 = \left[ \left( 1 - \sum_{i=1}^7 v_i \right) I + \sum_{i=1}^7 v_i A_i^{\text{dil}} \right]^{-1}, \quad \text{and}$$
 (8)

$$A_i^{\text{dil}} = [I + S_i C_{\text{polymer}}^{-1} (C_i - C_{\text{polymer}})]^{-1}. \tag{9}$$

- Here, I and S; are the identity tensor and the Eshelby tensor of region i, respectively.
- s In this study, only diagonal elements of the Eshelby tensors are considered due to
- the uniaxial loading condition. The diagonal elements can be calculated according to

$$S_{\text{diagonal}} - \frac{7 - 5vp}{15(1 - vp)}. \tag{10}$$

- The diagonal value along the C tensor is extracted as the effective elastic modulus.
- 11 Predictions of the effective elastic modulus from both simple tension simulation and
- MT method under different pyrolysis conditions are discussed in Sec. 3.1.

#### 3. Results and Discussion

13

14

15

16

19

20

21

22

24

25

26

27

28

**3.1.** Effect of pyrolysis parameters on the effective elastic modulus  $\boldsymbol{\mathsf{E}}$ 

Three sets of studies are carried out to evaluate the effect of holding time, heating rate andpyrolysis temperature on the effective elastic modulus of PDC composites. In the first set of this study, sample 1 to sample 3 are employed by considering different holding times of 1200 s, 1360s and 1700 s under the constant heating rate of 0.63 K/s and pyrolysis temperature of 1273K. The effective elastic modulus *E* is calculated according to the MT model, and the simple tension finite element model. The finite element predictions consider two scenarios: one scenario with each phase following idealized linear elastic constitutive law, and another scenario with each phase following the real constitutive law as shown in Fig. 5(b). It is noted from Fig. 7(a) that the number of co-existing phases decrease with the holding time. At 1200s, there are 2.4% of phase 2, 10.3% of phase 3, 60.4% of phase 4 and 26.9% of phase 5, respectively. When the holding time increases to 1360s, phase 2 disappears. The remaining phase 3, phase 4 and phase 5 are redistributed with the ratio of 2.7%, 9.7% and 87.6% instead. When the holding time increases to 1700s,

1

3

6

8

10

11

12

13

14

15

16

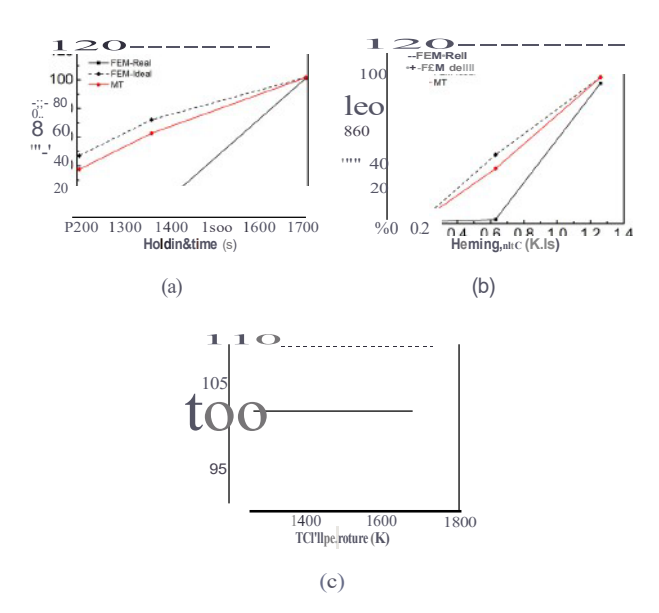
17

18

19

20

21



Fig, 6. Comparison of effective elastic modulus predicted from simple tension finite element simulation and MT approach under different (a) holding time, (b) heating rate and (c) pyrolysis temperature. The finite element predictions consider both idealized and realistic phase constitutive relationship.

only two phases exist i; mne percentttge of the sample has b rest of 1% stays in phase 5. As indicated to ceramic phase while 2022-07-18 15:42:47 the MT prediction is very close to the idealized FEM prediction, e longer holding time. However, the FEM prediction that employs the 99% tutive laws yields a much lower effective elastic modulus. This is because the MT model can only deal with two-phase linear elastic composite in a dilute situation. For multi-phase composites with different shapes or alignments of reinforcements, the MT solution becomes less accurate due to the violation of diagonal symmetry. internal-consistency and dilute requirements [Ferrari, 1991; Li, 1999]. Additionally the MT model does not consider the non-linear constitutive behaviors in PDC composites. Therefore, both the MT solution and the idealized FEM prediction would overestimate the effective elastic modulus in PDC composites, especially when the sample has more than two phases with low ceramic fraction phases being dominant. In two-phase composites with pure ceramics as the dominant phase, the three E predictions are reasonably close to each other according to Figs. 6(a) and 6(b).

It should be noted that the effective elastic modulus becomes independent of temperature when  $T \geq 1273 \, \mathrm{K}$  as shown in Fig. 6(c). This is because under the heating rate of  $0.63 \, \mathrm{K/s}$ , the sample can almost achieve full ceramization under pyrolysis temperature of 1273 K for 1700s. Further increase of pyrolysis temperature does not affect the ceramization process, leading to negligible change of elastic modulus as indicated in Fig. 7(c). This conclusion is consistent with the TGA

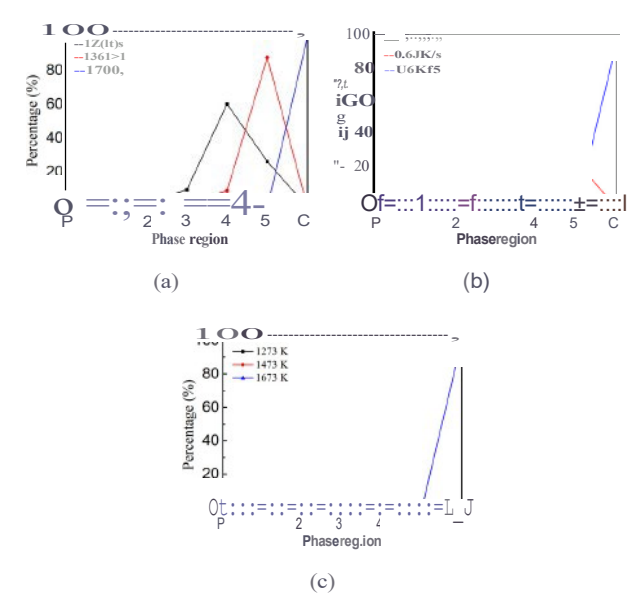


Fig. 7. Comparison of phase distribution under different (a) holding times, (b) heating rates and (c) pyrolysis temperatures.

analysis as the mass loss and ceramic yield remain unchanged once the temperature exceeds a certain threshold [Ma *et al.*, 2017a].

## **3.2.** Effect of pyrolysis parameters on fracture behaviors

1

2

3

4

6

7

10

11

12

13

14

15

16

17

1s

19

20

21

According to the discussion in Sec. 3.1, increase of holding time, heating rate and pyrolysis temperature before the threshold can lead to improved stiffness. In this section, effect of each processing parameter on the tensile fracture behavior is investigated. Figure 8(a) shows the stress-strain evolution during tensile deformation at various holding times when the heating rate of 0.63K/s and pyrolysis temperature of 1273 K are applied. At the holding time of 1200 s, the sample exhibits the most ductile behavior as its stress does not quickly drop to zero after reaching the peak. Instead, the sample can continue carrying load with additional stretch. As shown in Fig. 9(a), cracks start to initiate at the interface between phase 4 and phase 5 near the four sample corners. This is because a higher stress level is induced in phases with high ceramic fraction under the same amount deformation according to Fig. 5(b). Additionally, stress singularity that develops at the interface due to property mismatch promotes crack formation. Afterwards, the initiated cracks quickly propagate to phase 5, leading to an immediate stress drop from 19.18 MPa to 11.51MPa. It is noticed that further crack propagation tends to be along the interface at 0° plane which is perpendicular to the loading direction. The material is still able to regain strength as the emerged cracks are successfully bridged by the uncracked ligaments in phases 2, 3 and 4. Upon additional tension loading, new cracks are initiated in

2

3

4

S

6

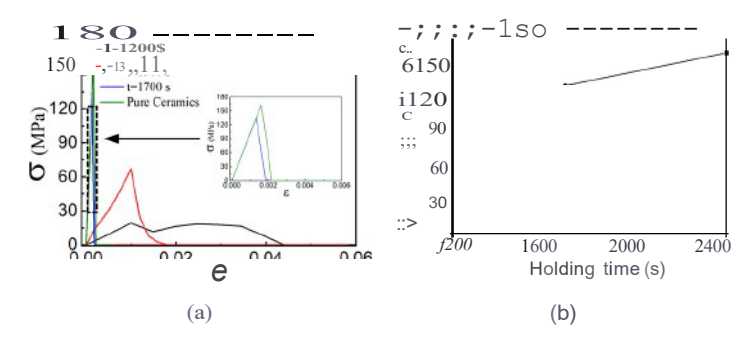


Fig. 8. (a) Stress-strain relationship and (b) ultimate strength of pyrolyzed samples under different holding times at temperature of 1273K and heating rate of 0.63K/s.

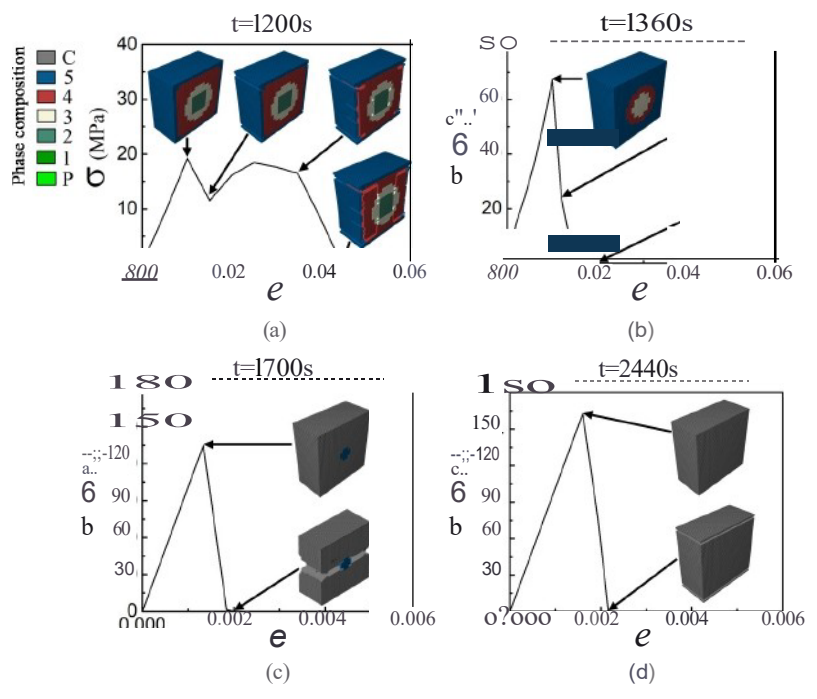


Fig. 9. Stress-strain curves with representative crack evolution snapshots at holding times of (a) 1200s, (b) 1360s, (c) 1700s and  $\{d\}$  2440s, respectively. Heating rate is kept at 0.63K/s with pyrolysis temperature of 1273K.

phase 5 near the sample center and along the interface between phase 3 and phase 4. The material completely loses its load bearing capacity when the new interfacial cracks coalesce with the existing cracks. When the holding time is increased to 1360s and 1700s, no corner cracks are observed as the interface location is further away from the corner as indicated in Figs. 9(b) and 9(c). Damages start to initiate at the interface located at the center of the sample and quickly propagate along the 0° plane. When the sample is fully converted to ceramics at 2440 s in Fig. 9(d),

1

2

3

4

10

11

12

13

14

1.5

16

17

18

19

20

21

22

23

24

25

26

27

28

30

31

32

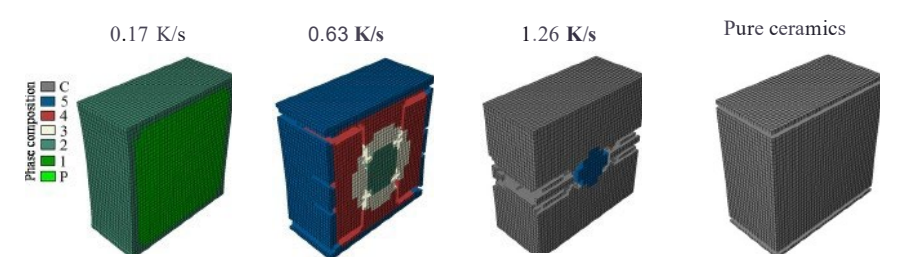


Fig. 10. Phase composition and damage distribution at various heating rates. Holding time is 1200s and pyrolysis temperature is 1273K.

fracture surfaces are perpendicular to the loading direction and are very close to the top and bottom planes due to the boundary constrains [Cordero *et al.*, 2014; Zhang *et al.*, 2018].

It is worth mentioning that, when multiple intermediate phases co-exist, damages are prone to initiate at the interface near the sample surface. Crack bridging is primarily achieved through intermediate phases with low strength. Therefore, both high strength and high ductility are difficult to achieve simultaneously under uniform heating. Similar crack patterns are observed in samples that are subject to varying heating rates. As shown in Fig. 10, no crack is observed at the heat rate of 0.17K/s when the holding time and pyrolysis temperature are kept at 1200s and 1273K. Only phase 1 and phase 2 exist in the sample. This type of composition can effectively mitigate the load without causing any damage. When heating rate increases to 0.63K/s, four intermediate phases co-exist in the sample. This phase composition yields a more complex fracture pattern due to the coalesce of interfacial cracks between phase 4-phase 5 and phase 2-phase 3. When the heating rate is further increased to 1.26K/s, the majority of the sample has been converted to pure ceramics. Its crack pattern is very similar to the case in Fig. 9(c). This indicates that a single intermediate phase, especially a high ceramic fraction phase, is not as effective as multiple intermediate phases in crack bridging. Pyrolysis temperature has the same impact on material strength and fracture behaviors when the heating rate and holding time are fixed.

It can be concluded from the above study that pyrolysis of preceramic polymers in a closed furnace cannot yield PDC composites with high strength, high ductility and high toughness at the same time. This is due to the inherent phase evolution under uniform heating. A fundamental avenue to achieve flexible property tailoring, especially controlled phase composition generation, would require gradient heating with precise temperature control capability. Laser pyrolysis is a potential way to generate predefined phase composition. Our future work will explore the effect of varying the processing parameters, such as laser powers, scanning speeds, and focus vs. defocus on PDC phase distribution and mechanical response. The computational work developed here provides a useful tool to predict the phase composition map in any PDC samples under arbitrary heating/cooling histories.

#### 4. Summary

A multiscale computational model is developed to find the relationship among pyrolysis condition, phase transition and mechanical tensile response of PDC composites. The macroscale phase distribution is determined from the interplay between gas generation and gas diffusion. This model allows phase composition distribution to be explicitly extracted from arbitrary processing routes. The phase composition map serves as the input for finite element analysis. It is found that the MT model can only predict the effective elastic modulus in two-phase PDC composites under 8 dilute situation. Property predictions in multi-phase or non-dilute two-phase PDC 10 composites require advanced constitutive modeling in the intermediate phases. In this work, the constitutive law of each intermediate phase is determined through 11 both experiment and simple tension simulation. It is found that the phase com-12 position has a significant impact on the stiffness and strength of PDC composites. Microcracks tend to initiate at the interface between intermediate phases, espe-14 cially those with ceramic fraction greater than 60%. Although intermediate phases 15 with low ceramic fraction (<40%) can avoid microcrack formation, they cannot promote material strengthening due to their own low strengths. It is found that the 17 optimized phase composition that can effectively bridge cracks without scarifying 18 strength cannot be achieved through uniform heating in a closed furnace. A more 19 advanced pyrolysis design is required for achieving PDC composites with both high 20 strength and toughness. 21

## 22 Acknowledgment

- The authors acknowledge the support from NH BioMade Project which is provided by the National Science Foundation's Research Infrastructure Improvement Award # 1757371, as well as the start-up funds from the Thayer School of Engineering at
- 26 Dartmouth College.

## References

21

28

29

30

35

36

37

- Alizadeh-Osgouei, M., Li, Y. and Wen, C., [2018) "A comprehensive review of biodegradable synthetic polymer-ceramic composites and their manufacture for biomedical applications," *Bioact. Mater.* **4**, 22-36.
- Bernard, S., Fiaty, K., Comu, D., Miele, P. and Laurent, P., [2006) "Kinetic modeling of the polymer-derived ceramics route: Investigation of the thermal decomposition kinetics of poly[B-(methylamino)borazine) precursors into boron nitride," J. *Phys. Chem. B* **110**, 9048-9060.
  - Colombo, P., Riedel, R., Soraru, G. D. and Kleebe, H. K. [2009) "Historical review of the development of polymer derived ceramics (PDCs)," *Polymer Dervied Ceramics: From Nanostructure to Apllications.* DEStech Publications Inc., pp. 1-12.
- Cordero, Z. C., Huskins, E. L., Park, M., Livers, S., Frary, M., Schuster, B. E. and Schuh, C. A., [2014) "Powder-route synthesis and mechanical testing of ultrafine grain tungsten alloys," *Metal. Mater. Trans. A* 45, 3609-3618.

- Eckel, Z. C., Zhou, C., Martin, J. H., Jacobsen, A. J., Carter, W. B. and Schaedler, T. A., [2016] "Additive manufacturing of polymer-derived ceramics," *Science* 351, 58-62.
- Ferrari, M., (1991] "Asymmetry and the high concentration limit of the Mori-Tanaka effective medium theory," *Me.ch. Mater.* 11, 251-256.
  - Fisher, F. T. and Brinson, L. C., [2006] "Nanomechanics of nanoreinforced polymers," *Handbook of Theoretical and Computational Nanoscience*. American Scientific Publishers, pp. 253-360.
  - Gonzalez, J., Cano, S., Schuschnigg, S., Kukla, C., Sapkota, J. and Holzer, C., [2018] "Additive manufacturing of metallic and ceramic components by the material extrusion of highly-filled polymers: A review and future perspectives," *Materials* 11, 840.
  - Gottardo, L., Bernard, S., Gervais, C., Weinmann, M. and Miele, P., [2012] "Study of the intermediate pyrolysis steps and mechanism identification of polymer-derived SiBCN ceramics," *J. Mater. Chem.* **22**, 17923--17933.
  - Justin, J. F. and Jankowiak, A., [2011] "Ultra High Temperature Ceramics: Densification, Properties and Thermal Stability," AerospaceLab, p-1.
    - Kim, T. K., Kim, J. K. and Jeong, O. C., [2011] "Measurement of nonlinear mechanical properties of PDMS elastomer," *Microelectron. Eng.* **88**, 1982-1985.
    - Konstantinou, G., Kakkava, E., Hageliiken, L., Sasikumar, P. V. W., Wang, J., Makowska, M. G., Blugan, G., Nianias, N., Marone, F. and VanSwygenhoven, H., [2020] "Additive micro-manufacturing of crack-free PDCs by two-photon polymerization of a single, low-shrinkage preceramic resin," *Additive Manuf.* 35, 101343.
    - Kulkarni, A. D., Truhlar, D. G., Goverapet Srinivasan, S., Van Duin, A. C. T., Norman, P. and Schwartzentruber, T. E., [2013] "Oxygen interactions with silica surfaces: Coupled cluster and density functional investigation and the development of a new ReaxFF potential," *J. Phys. Chem. C* 117, 258-269.
    - Lee, D., [2018) "Local anisotropy analysis based on the Mori-Tanaka model for multiphase composites with fiber length and orientation distributions," *Composites Part* B: *Engineering* **148**, 227-234.
    - Li, J. Y., [1999) "On micromechanics approximation for the effective thermoelastic moduli of multi-phase composite materials," *Mech. Mater.* **31**, 149--159.
    - Li, R., Hou, P., Xie, N., Ye, Z., Cheng, X. and Shah, S. P., [2018a) "Design of SiO2/PMHS hybrid nanocomposite for surface treatment of cement-based materials," *Cement Concrete Compos.* 87, 89--97.
    - Li, Y. J., Fan, C. Y., Zhang, J. P. and Wu, X. L., [2018b] "A promising PMHS/PEO blend polymer electrolyte for all-solid-state lithium ion batteries," *Dalton Trans.* 47, 14932-14937.
    - Lu, X., Wang, X., Li, Q., Huang, X., Han, S. and Wang, G., [2015] "A ReaxFF-based molecular dynamics study of the pyrolysis mechanism of polyimide," *Polym. Degmd. Stab.* **114**, 72-80.
    - Ma, B., Cao, Y., Gao, Y. and Wang, Y., [2017a] "Fabrication of a thin double-layer thermistor based on DVB-modified polymer-derivedSiCN ceramics," *J. Alloys Compounds* 732.
  - Ma, C., Ji, T., Robertson, C. G., Rajeshbabu, R., Zhu, J. and Dong, Y., (2017b) "Molecular insight into the Mullins effect: Irreversible disentanglement of polymer chains revealed by molecular dynamics simulations," *Phys. Chem. Chem. Phys.* 19, 19468-19477.
- Ma, C. and Li, Y., [2021] "Modeling of phase transition in fabrication of polymer-derived ceramics (PDCS)," *Int. J. Comput. Mater. Sci. Eng.* 11, 2150032.
- Merkel, T. C., Bondar, V. I., Nagai, K., Freeman, B. D. and Pinnau, I., (2000] "Gas sorption, diffusion, and permeation in poly(dimethylsiloxane)," *J. Polym. Sci. B Polym.* so *Phys.* **38**, 415-434.

6

8

9

10

11

12

13

14

15

16

17

18 19

20

21

22

23 24

25

26

29 30

31

32

33

- Plimpton, S., [1995] "Fast parallel algorithms for short-range molecular dynamics," *J. Comput. Phys.* 117, 1-19.
- Ponomarev, I., Van Duin, A. C. T. and Kroll, P., [2019] "Reactive force field for simulations of the pyrolysis of polysiloxanes into silicon oxycarbide ceramics," *J. Phys. Chem. C* **123**, 16804-16812.
  - Sorarii., G. D., Kundanati, L., Santhosh, B. and Pugno, N., [2019] "Influence of free carbon on the Young's modulus and hardness of polymer-derived silicon oxycarbide glasses," *J. Am. Ceram. Soc.* 102, 907-913.
    - Stabler, C., Reitz, A., Stein, P., Albert, B., Riedel, R. and Ionescu, E., [2018] "Thermal properties of SiOC glasses and glass ceramics at elevated temperatures," *Materials* 11, 279.
    - Thorvaldsen, T., (2015] "Modelling the elastic stiffness of nanocomposites using the Mori-Tanaka method."
      - Venkatachalam, S. and Hourlier, D., (2019] "Heat treatment of commercial Polydimethylsiloxane PDMS precursors: Part I. Towards conversion of patternable soft gels into hard ceramics," *Ceram. Int.* 45, 6255-6262.
  - Vozza, A., [2021] Mechanical Properties and Spectral Vibrational Response of Si-O-C With and Without Graphene Toughening. University of Central Florida.
  - Vry, S., Roumanie, M., Laucournet, R. and Bernard-Granger, G., (2020] "Transmission electron microscopy investigations on a polysiloxane preceramic polymer pyrolyzed at high temperature in argon," *Ceramics* 3, 421-427.
  - Waku, Y., Nakagawa, N., Wakamoto, T., Ohtsubo, H., Shimizu, K., Kohtoku, Y., [1997] "A ductile ceramic eutectic composite with high strength at 1,873 K," *Nature* 389, 49-52.
    - Wan, J., Gasch, M. J. and Mukherjee, A. K., [2004] "InSitu densification behavior in the pyrolysis consolidation of amorphous Si-N-C bulk ceramics from polymer precursors," *J. Am. Ceram. Soc.* 84, 2165-2169.
    - Wei, T., Yan, F. and Tian, J., [2005] "Characterization and wear-and corrosion-resistance of microarc oxidation ceramic coatings on aluminum alloy," *J. Alloys Compounds* **389**, 169-176.
    - You, X., Hu, Q., Hu, X., Chen, H., Yang, W. and Zhang, X., (2019] "An effective, economical and ultra-fast method for hydrophobic modification of NCC using poly(methylhydrogen) siloxane," *Polymers* 11, 963.
- Zhang, P., Li, S. X. and Zhang, Z. F., [2011] "General relationship between strength and hardness," *Mater. Sci. Eng. A* 529, 62-73.
- Zhang, X., Mu, Y., Dodaran, M., Shao, S., Moldovan, D. and Meng, W. J., (2018] "Mechanical failure of CrN/Cu/CrN interfacial regions under tensile loading," *Acta Mater.* 160, 1-13.